

STUDY FOR AN EP INSTABILITY IN THE JOINT PROJECT OF KEK AND JAERI

T. Toyama, Y. Irie, S. Kato, K. Ohmi, C. Ohmori, K. Satoh and M. Uota

KEK, Oho, Tsukuba, Ibaraki 305-0801, Japan

N. Hayashi

JAERI, Tokai, Naka, Ibaraki 319-1195, Japan

Abstract

An e-p instability has been observed in some proton rings. This instability, which causes beam loss, limits the performance of the ring. The instability may be serious for 3 GeV and 50 GeV proton rings in JKJ. We have studied the e-p instability in several high-intensity proton rings: JKJ, PSR, ISIS and AGS. This work informs JKJ whether we have to take measures to cure the instability. A TiN coating on the chamber surface is one of remedies. Results of SEY measurements performed at KEK are discussed. The observation of electron cloud candidates at the KEK 12 GeV PS Main Ring is also presented.

1 INTRODUCTION

A high-intensity proton accelerator facility has been proposed in Japan as a joint project of KEK and JAERI (JKJ). The facility would be equipped with two proton rings: a 3 GeV rapid cycling synchrotron and a 50 GeV proton synchrotron [1]. The bunch population, which would be 4×10^{13} , compares with that of PSR at Los Alamos National Laboratory [2]. The e-p instability is potentially a serious problem for these two rings of JKJ.

Not all high-intensity proton rings suffer from an electron cloud instability. For example, the instability has not been observed at a rapid cycling synchrotron, ISIS in Rutherford Appleton Laboratory [3], although it has an intensity comparable with PSR. AGS in Brookhaven National Laboratory has intensity with only a few factor difference of the JKJ 50 GeV ring. However, the instability has not been observed yet [4]. It is worth comparing these proton rings from the viewpoint of the electron cloud instability. The parameters of these proton rings are summarized in Table 1 [5].

The electron cloud could cause both coupled and single bunch instabilities. A perturbation of the cloud induced by a bunch, which affects other bunches, causes a coupled bunch instability. A perturbation induced by a part of a bunch, which affects other part of the bunch, causes a single bunch instability. In these rings, both the bunch length and the bunch spacing are several tens meters. At first sight, a bunch spacing of several tens meters seems to be long enough to decay the perturbation (wake field) of a bunch. We focus on the single bunch instability in this paper. The coupled bunch effect will be discussed at some other opportunity.

The 50 GeV ring in JKJ should supply not only a fast-extracted beam, but also a slow-extracted beam. An electron cloud build-up and an instability of a coasting proton beam would occur in somewhat different ways, which is not covered here, although it is very crucial.

It is important to know the secondary electron yield efficiency (SEY) not only as a candidate of remedies, but also as an input of a computer simulation. The results of ongoing measurements of SEY at KEK are discussed for several materials. The observation of electron cloud candidates at the KEK 12 GeV PS Main Ring is also discussed as a benchmark of the computer simulation, although not yet confirmed.

2 FORMATION OF AN ELECTRON CLOUD

In this section, the electron cloud density of each ring is evaluated based on a computer simulation considering the primary and secondary electrons.

Three possibilities of primary electron production are considered: i.e. the ionization of residual gas due to the proton beam, electron emission due to protons impinging on the vacuum chamber wall, and stripping at the foil for H-minus charge exchange injection.

The ionization cross-sections for CO and H₂ are estimated to be $\sigma(\text{CO}) < 1.3 \times 10^{-22} \text{ m}^2$ and $\sigma(\text{H}_2) < 0.3 \times 10^{-22} \text{ m}^2$ using Bethe formula. The molecular density (d_m) is related to the partial pressure in nPa by the relation at 20 °C, $d_m(\text{m}^{-3}) = 2.4 \times 10^{11} P_m$ (nPa). The electron production rate is $Y_{1,i} = 7.7 \times 10^{-9} \text{ e}^-/(\text{m}\cdot\text{p})$ at $2 \times 10^{-7} \text{ Pa}$, where $\text{e}^-/(\text{m}\cdot\text{p})$ means the number of emitted electrons per one proton incident per meter.

On the other hand the electron production rate due to proton loss is assumed to be $Y_{1,\ell} = 4.4 \times 10^{-6} \text{ e}^-/(\text{m}\cdot\text{p})$ at the chamber surface, assuming a proton loss rate of 4×10^{-6} per revolution and one hundred electron emissions per one proton loss. Here, the assumption of M. Furman et al. [6] is adopted. The electron production rate due to proton loss is a third order of magnitude larger than that due to ionization.

Electrons stripped at the foil have a kinetic energy of 217 keV during H-minus charge-exchange injection. The leakage magnetic fields of bump magnets is estimated to be larger than 20 G around the foil. Almost all of the

Table 1. Basic parameters of the proton rings.

Variable	symbol	Joint project				PSR	ISIS	AGS
		3GeV RCS		50GeV MR				
		inj.	ext.	inj.	ext.		inj.	inj.
circumference	L(m)	348.3	348.3	1567.5	1567.5	90	163	800
Lorentz factor	γ	1.4	4.2	4.2	54	1.85	1.07	3.0
Bunch population	$N_p(\times 10^{13})$	4.15	4.15	4.15	4.15	3	1.25	1.2
Number of bunches	n_b	2	2	8	8	1	2	6
Harmonic number	h	2	2	9	9	1	2	6
Rms beam size	$\sigma_r(\text{cm})$	1.9	1.2	1.1	0.35	1.0	3.8	0.7
Bunch length	$\ell_p(\text{m})$	110	82	82	16	65	60	68
Rms energy spread	$\sigma_E/E(\%)$	0.6	0.7	0.7	0.25	0.25	0.025	0.28
Slippage factor	η	-0.48	-0.047	-0.058	-0.0013	-0.187		-0.146
Synchrotron tune	Q_s	0.0058	0.0005	0.0026	0.0001	0.0003		0.0017
Beam pipe radius	R(cm)	12.5	12.5	6.5	6.5	5	8	5

stripped electrons will be bent by these fields. The electron production rate is $2 \times N_p / T_{\text{rev}} \sim 5.4 \times 10^{11} \text{ e}^-/\text{turn}$. Converting into the electron yield per one proton incident per meter reads $Y_{1,\text{foil}} = 1.9 \times 10^{-5} \text{ e}^-/(\text{m} \cdot \text{p})$. This value is four times larger than $Y_{1,e}$. These electrons, however, may not cause big trouble, because (1) primary electrons of 217 keV are swept from the beam orbit, and (2) secondary electrons of a few tens eV are easily localized by the leakage fields.

In the simulation, therefore, electron production due to proton loss dominates the electron cloud build-up.

The secondary electron yield, which is the number of electrons created by an electron incidence with some energy, is approximated by true secondary electron yield, as follows [7, 8]:

$$Y_2 = Y_S \times \frac{E}{E_{\text{max}}} \frac{1.44}{0.44 + (E/E_{\text{max}})^{1.44}}.$$

$Y_S=2.1$ and $E_{\text{max}}=200 \text{ eV}$ are used. Rediffused and elastic reflected electrons are not included in this simulation. SEY is varying in a practical situation, depending on materials, surface conditions and so on. Simple aspect is as follows. If an electron hits the wall n times on average, multiplication will amount to Y_2^n . Taking into account $n=10-100$ per one bunch passage, it is easily seen that a small change in Y_2 causes a large multiplication. This shows the importance of reducing SEY.

Electron cloud formation is estimated by tracking the transverse 2D motion of electrons produced by the primary and secondary electron emission. Primary electrons are produced at the chamber wall with energies of $10 \pm 5 \text{ eV}$. At position s along the ring, electrons move under an electric potential generated by a rigid proton beam of sinusoidal shape ($\lambda_p(s-vt) = (\pi N_p / 2\ell_p) \sin(\pi(s-vt)/\ell_p)$). Space charge force between electrons is neglected because the average neutralization factor is

less than 0.1 in the rings discussed here. The magnetic fields are also neglected in the whole ring for simplicity.

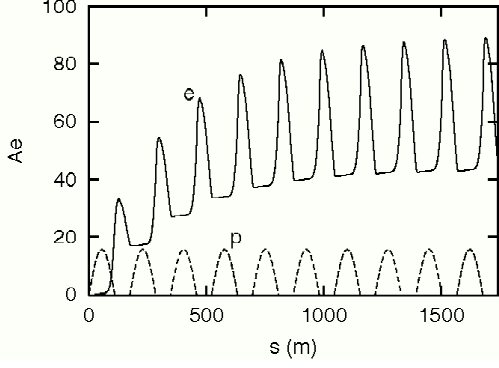
The amplification factor (A_e), the number of multiplied electrons divided by the number of primary electrons per one bunch passage, is calculated for several stages of the relevant rings using the parameters in Table 1. The results are shown in Figure 1. This characterizes the amplification factor due to secondary electron emission. At every bunch passage a peak is formed by trailing-edge multipacting. Although it decays after the bunch passage, a considerable rate of electrons remains in the vacuum chamber upon the arrival of the next bunch. The base line increases as remaining electrons accumulate. Finally equilibrium is reached in 5 – 10 bunches passage. The peak and bottom values of the amplification factor and the neutralization factor are summarized in Table 2. The neutralization factor strongly depends on several parameters: the beam size, chamber size, bunch length and bunch spacing.

3 INSTABILITY CAUSED BY AN ELECTRON CLOUD

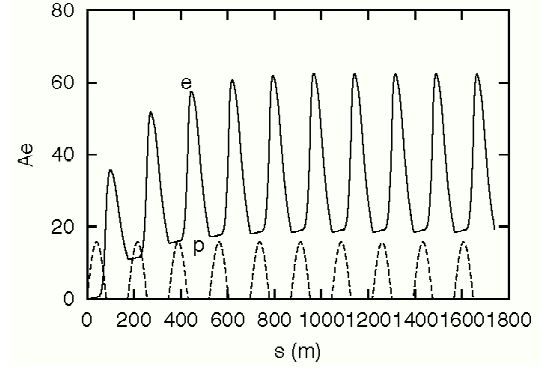
In this section the beam stability is evaluated based on a wake field approach and a coasting beam approximation because $\omega_e \sigma_z/c \gg 1$ and the instability may be fast enough regardless of the synchrotron oscillation. Both the proton beam and the electron cloud are assumed to have a rigid Gaussian distribution. By linearizing the coupled motion, the proton motion can be considered to be a forced oscillation with the wake field that is generated by the proton beam passing through the electron cloud. Including the damping effect due to electron oscillation frequency spread, the wake is expressed as [9,10]

$$W(z) = c \frac{R_s}{Q} \frac{\omega_e}{\bar{\omega}} \exp\left(\frac{\alpha}{c} z\right) \sin\left(\frac{\bar{\omega}}{c} z\right),$$

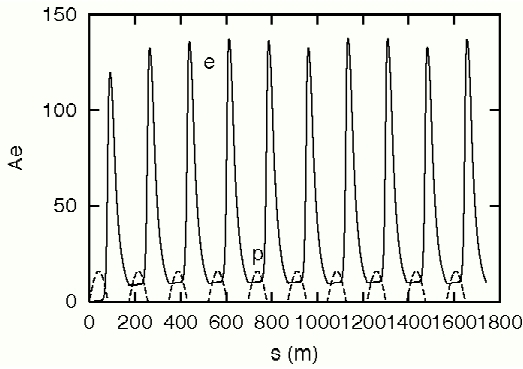
Joint project (JKJ) / 3 GeV RCS
@Injection



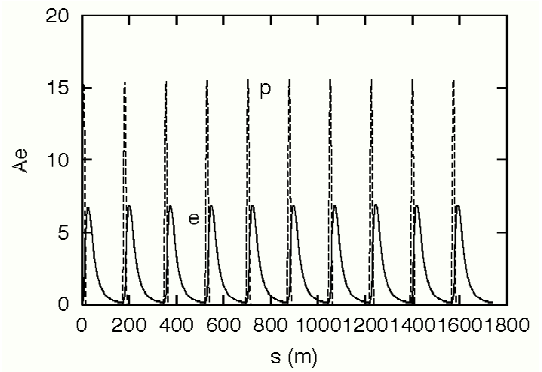
@Extraction



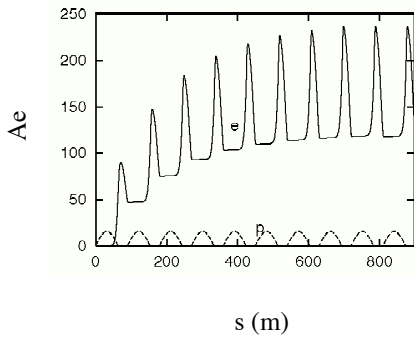
Joint project (JKJ) / 50 GeV MR
@Injection



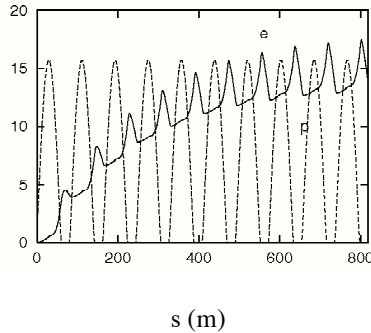
@Extraction



PSR



ISIS @Injection



AGS @Injection

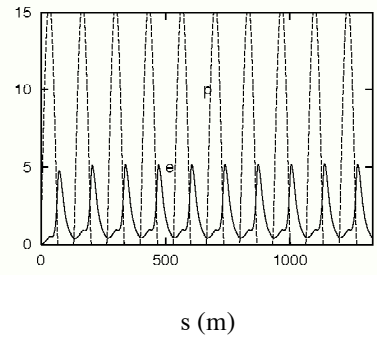


Figure 1. Electron amplification factor and proton beam density for the JKJ 3 GeV RCS, 50 GeV MR, PSR, ISIS and AGS. The dashed curves are the proton beam densities of a “half-sin” bunch (arbitrary unit). The parameters listed in Table 1 were used for the simulation.

Table 2. Electron cloud build-up of the proton rings.

Variable	Joint project				PSR	ISIS	AGS
	3 GeV RCS inj.	ext.	50 GeV inj.	MR ext.			
Ae(bottom)	42.0	18.0	9.4	0.13	118	12.9	0.42
Ae(peak)	87.6	62	136	6.9	236	17.5	5.18
η (bottom)	0.020	0.0067	0.0035	0.00001	0.034	0.003	0.0001
η (peak)	0.042	0.023	0.05	0.0005	0.067	0.005	0.0015

Table 3. Wake field and stability for the electron cloud instability.

Variable	Joint project				PSR	ISIS	AGS
	3 GeV RCS inj.	ext.	50 GeV MR inj.	ext.			
$Z(\omega_e)_L/Q$ (M Ω /m)	0.29	0.24	0.68	0.019	0.46	0.0051	0.024
$Z(\omega_e)_H/Q$ (M Ω /m)	0.61	0.83	9.7	0.96	0.90	0.0085	0.37
$\omega_e \ell_p / c$	133	182	199	276	166	27	153
U_L	0.07	0.23	0.11	0.02	1.6	0.09	0.004
U_H	0.23	0.78	1.6	1.2	3.2	0.14	0.06

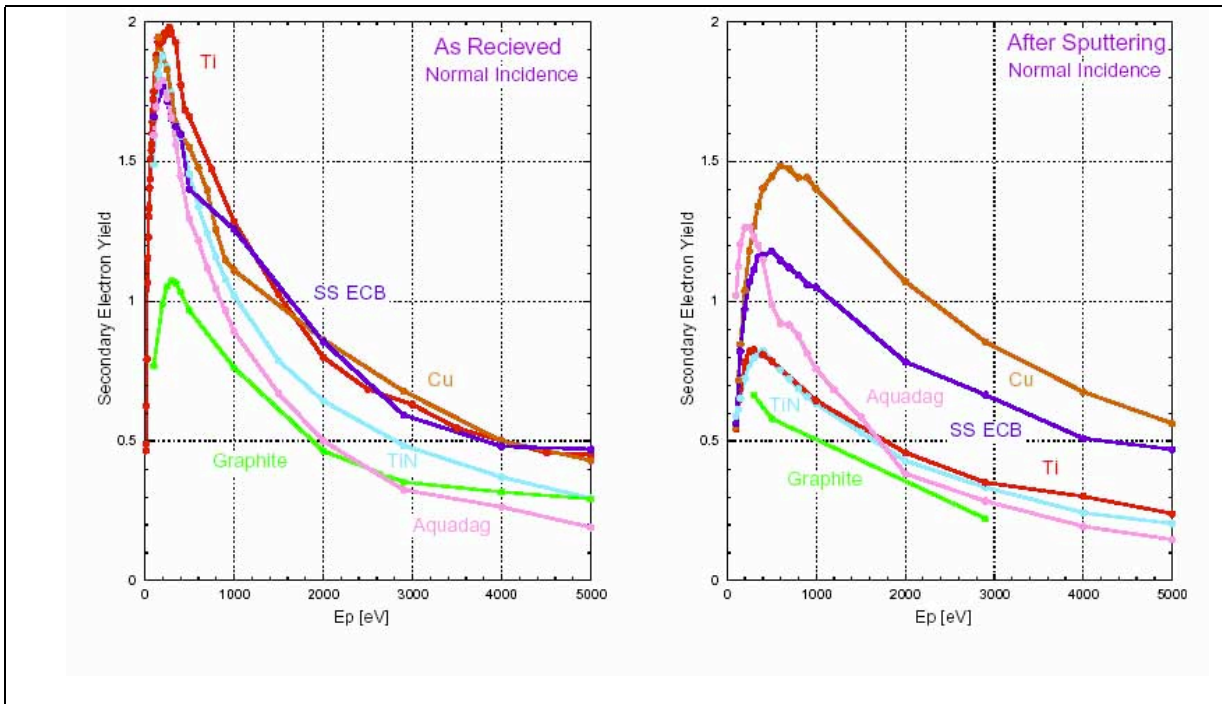


Figure 2. Dependence of the secondary electron yields on the primary electron energies at the surface as-received and after sputtering.

$$\begin{aligned}
c &: \text{light speed,} \\
R_s &: \text{shunt impedance,} \\
Q &: \text{quality factor,} \\
\omega_e &: \text{resonance angular frequency,} \\
\alpha &= \omega_e / 2 Q, \\
\bar{\omega} &= \sqrt{\omega_e^2 - \alpha^2}.
\end{aligned}$$

Corresponding transverse impedance is given by Fourier transformation of the wake field:

$$Z_{\perp}(\omega) = \frac{Z_0}{4\pi} \frac{\lambda_e}{\lambda_p} \frac{L}{2\sigma_r^2} \frac{\omega_e}{\omega} \frac{Q}{1 + iQ\left(\frac{\omega_e}{\omega} - \frac{\omega}{\omega_e}\right)},$$

$$\begin{aligned}
Z_0 &: \text{vacuum impedance,} \\
\lambda_e &= \text{line density of the electron cloud,} \\
\lambda_p &= \text{line density of the proton beam,} \\
L &: \text{circumference} \\
\sigma_r &: \text{rms bunch radius.}
\end{aligned}$$

Making use of this coupling impedance, the dispersion relation is obtained [11, 12]:

$$U \equiv \frac{\sqrt{3}\lambda_p r_0 \beta_r \omega_0}{\gamma \omega_e \eta \sigma_{\delta}} \frac{|Z_{\perp}(\omega_e)|}{Z_0} = 1$$

or

$$\frac{\sqrt{3}\lambda_p r_0 \beta_r}{\gamma v_s \omega_e \sigma_z / c} \frac{|Z_{\perp}(\omega_e)|}{Z_0} = 1$$

$$\begin{aligned}
r_0 &: \text{classical radius of protons,} \\
\beta_r &: \text{betatron function} \\
\gamma &: \text{relativistic factor,} \\
\eta &: \text{phase slip factor,} \\
\sigma_{\delta} &: \text{relative energy rms spread,} \\
\sigma_z &: \text{bunch length.}
\end{aligned}$$

For $U > 1$, the beam is unstable. In Table 3, two values of U_H and U_L are listed. They are unstable criteria for the peak and bottom values of the neutralization factor, respectively. For ISIS, the slippage factor and the synchrotron tune are assumed to be the same as PSR. PSR is unstable. On the other hand, ISIS and AGS are stable. These results qualitatively agree with the observations. The rings of the joint project are in-between.

4 SEY MEASUREMENTS

In this section, the results of ongoing measurements of SEY at KEK are discussed for several materials. A series of measurements of the secondary electron yields were made using an electron beam of 0.5 mm in diameter with an energy range of 100 to 5000 eV and a current of some tens nA, or using an argon ion beam with a raster-scanned size of a few mm², an energy of 5000 eV and a current of some tens nA. Surfaces of sample materials were analysed with x-ray photoelectron spectroscopy (XPS) or Auger electron spectroscopy (AES). The base

pressure of the main chamber where all of the measurements were performed was close to 10⁻⁸ Pa. A detailed description of the experiment is reported in [13].

Figure 2 shows the dependence of the secondary electron yields on the primary electron energy with normal incidence at the as-received surfaces and after sputtering with argon ions. Although a titanium as-received sample showed the highest yield, the yields of the others, except an isotropic graphite, were close to the peak of titanium, as seen on the left. At a high energy region, the yields of the metals as-received appeared to be similar. However, the yields of the carbon materials and the TiN film showed lower. The yields of the all materials were reduced after the argon ion sputtering. The isotropic graphite showed the lowest value of 0.66 as well, even after slight sputtering, reaching almost its clean surface. Since the carbon and oxygen impurities in the TiN film reached their saturation and remained even after sputtering of a thickness of 65nm, those impurities may have been included in the film, itself, during its preparation. Their reduction may reduce the yields of TiN further.

The simulation here doesn't reflect the above results yet. Further investigation on electron cloud build-up will be performed by using these results.

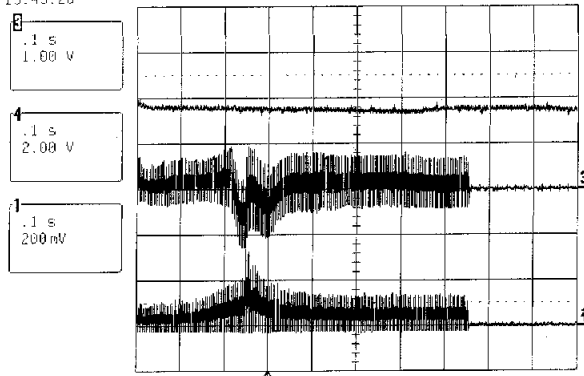
5 ELECTRON CLOUD IN THE KEK-PS

There had been no evidence of electron cloud effects in the KEK-12 GeV-PS Main Ring. This January electrostatic pick-ups were installed in the MR to measure the transverse monopole, dipole and quadrupole component of the beam [14]. Four electrodes for monopole (by Σ) and quadrupole measurement were directly connected to the center control room on trial. Although a 50 ohm termination is normal, the measurement with a high impedance termination was intentionally performed to observe an electron cloud. Baseline drifts were observed around the transition energy and around the beginning of the flat top even at a relatively low intensity operation of 2.5×10^{12} protons per pulse (9 bunches), as shown in Fig. 3. The rf frequency sweeps from 6 MHz to 8 MHz. The full bunch length varies from ~ 90 ns at injection to ~ 30 ns at transition energy. The top trace is the number of particles, the middle trace a pick-up signal and the bottom trace the bunch signal from a wideband wall current monitor (WCM) in each figure. The envelope of the WCM signal peaks at the transition energy. With a 50 ohm termination the pick-up signal has a similar shape as the WCM signal. This implies a charge-up of the pick-ups with a negative current of a few microamperes.

Although there seems to be no instability and no problem for operation, the following experiments were performed to clarify the source of the baseline drift: baseline drift vs. bias voltage with various bunch numbers and with or without a magnetic solenoid field. The first idea was that it came from some resonance of the system because a preferred frequency seems to exist.

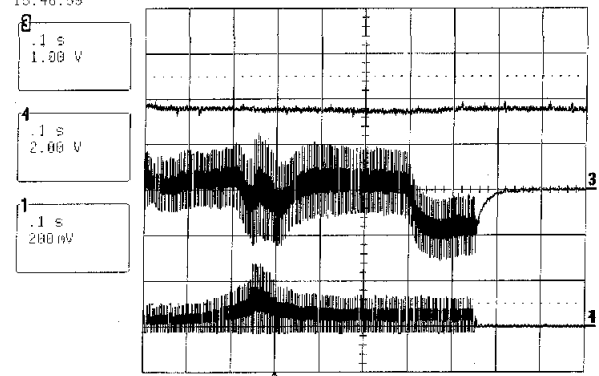
Upper electrode

17-Mar-02
15:45:28



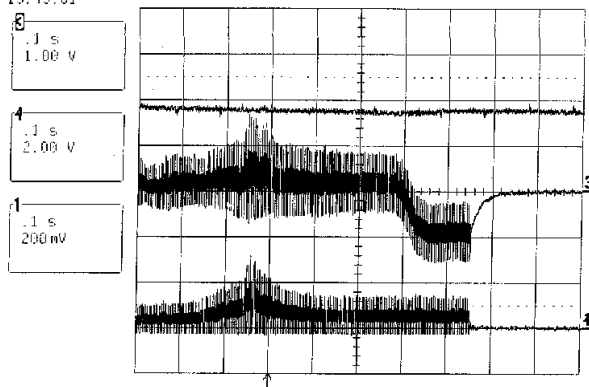
Left electrode (outer side of the ring)

17-Mar-02
15:46:59



Lower electrode

17-Mar-02
15:49:01



Right electrode (inner side of the ring)

17-Mar-02
15:50:34

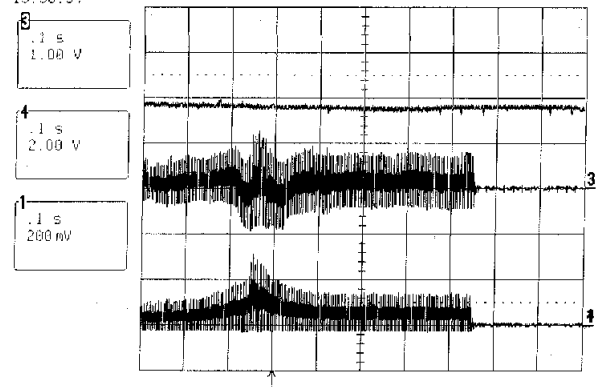


Figure 3. Baseline drifts around the transition energy and around the beginning of the flat top at a relatively low intensity operation of 2.5×10^{12} protons per pulse (9 bunches). Trigger: 400 ms after the beginning of acceleration indicated by the arrow. The transition energy is ~ 350 ms after the beginning of acceleration.

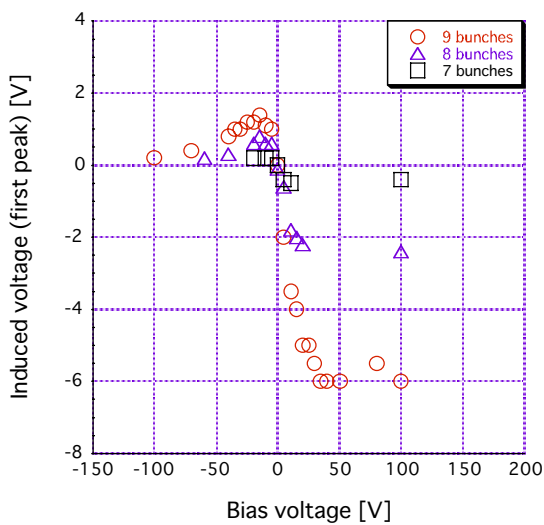


Figure 4. Peak voltage of the baseline drift at the transition energy with the number of bunches (7, 8 and 9).

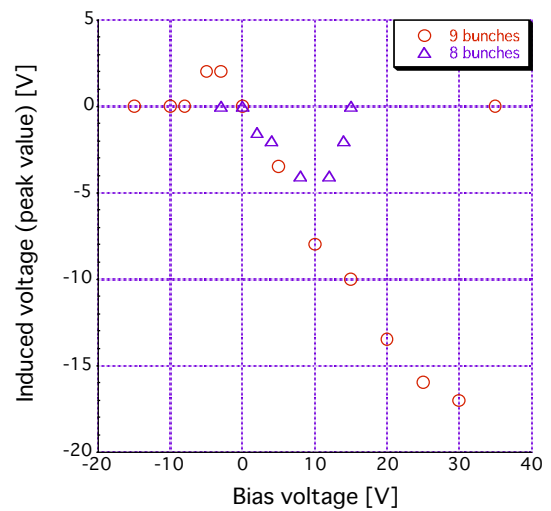


Figure 5. At a fixed bunch number 9, the peak voltage of the baseline drift measured with the solenoid current of 0, 10, 20 and 30 A.

If it comes from some geometrical reason, there may be no saturation. On the other hand, if it comes from electrons, there may be saturation.

Figure 4 shows the peak voltage of the baseline drift at the transition energy with seven, eight or nine successive bunches. The baseline drift was saturated by applying more than ~ 40 V of positive bias. With increasing the negative bias, the baseline once increases and then decreases, and gradually approaches to zero. This saturation level decreased with increasing bunch gap. In this measurement the bunch population was kept at 2.8×10^{11} protons. The baseline drift was not detectable if the bunch number was less than 6.

At a fixed bunch number of 9, the peak voltage of the baseline drift was measured with solenoid currents of 0, 10, 20 and 30 A, as shown in Fig. 5. The field distribution at 25 A is plotted in Fig. 6, more than 25 G at the vacuum chamber surface. The Lamor radius at 300 eV electron is ~ 23 mm at 25 G, which can force electrons away from the beam.

Although the above experiments do not contradict the statement that the baseline drift comes from the electron cloud, further study is necessary to confirm it.

To get an impression, the electron build-up was calculated with the beam parameters of the experiments. The simulation was basically the same as that described in the previous section. The only difference is that the effect of reflected electrons was checked. The results were quite different whether elastic reflected electrons

were included or not, as shown in Fig. 7. Without elastic reflected electrons, A_e is ~ 7 , while including them causes a large A_e of more than 260, not saturated yet, as shown in Fig. 7. Elastic reflection may lengthen the electron lifetime and make A_e larger. Introducing an electron space charge may work in the opposite way, i.e. to suppress electrons generation.

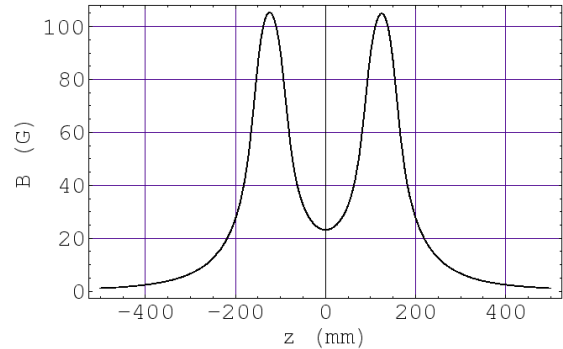


Figure 6. Magnetic fields at the vacuum chamber surface at a current of 25 A. The pick-up of 300 mm in length is located at $|z| < 150$ mm.

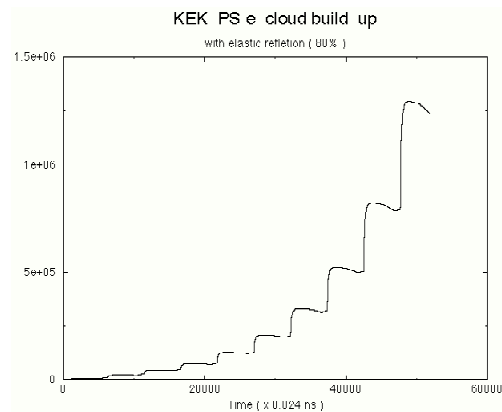
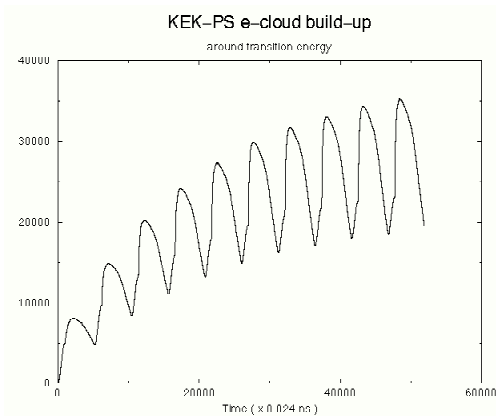


Figure 7. Simulation of electron build-up around the transition energy. Primary electrons of 5000 are generated at every bunch passage. The left plot is only with true secondary electrons. In addition, the right plot includes elastically reflected electrons.

6 SUMMARY

Electron cloud build-up and beam stability were evaluated for high intensity proton rings: JKI 3 GeV

RCS, 50 GeV MR, LANL PSR, RAL ISIS and BNL AGS. The assumptions in the simulation were as follows: estimated in field free region, included only true secondary electrons, without space charge effect. The number of primary electrons is amplified by

trailing-edge multipacting. The rate strongly depends on the secondary electron yield, beam shape, and chamber geometry. Then, using the neutralization factor obtained by the simulation, the beam stability was evaluated using a coasting beam model. The obtained stabilities agree qualitatively with observations in the existing machines. The neutralization factor due to the electron cloud was less than 0.1, neglecting elastic reflection in the secondary electron emission and electron space charge. This low neutralization degree justifies the neglecting electron space charge. However, including the elastic reflection in the secondary electron emission raises the neutralization factor by more than one order of magnitude. Including both the elastic reflection and the electron space charge may tend to cancel each other. This is a subject for future study.

A low SEY material, such as TiN, may improve the stability, if surface processing is carefully performed. Further experiments, including *in situ* measurement with several materials are foreseen, if the described baseline drift phenomena at the pickups in KEK-PS are confirmed to be the result of an electron cloud effect.

7 REFERENCES

- [1] JAERI/KEK Joint Project Team, Accelerator Technical Design Report for High-Intensity Proton Accelerator Facility Project, .
- [2] R. J. Macek et al., Proc. of Part. Acel. Conf. 2001, p. 688.
- [3] G. H. Rees, AIP Proceedings 496 (1999) p. 17.
- [4] T. Roser, AIP Proceedings 496 (1999) p. 22.
- [5] C. Ohmori,
<http://hadron.kek.jp/member/chihiro/ep.html>, (in Japanese).
- [6] M. A. Furman and M. Pivi, Proc. of Part. Acel. Conf. 2001, 707.
- [7] M. A. Furman and G. R. Lanbertson, Proc. Intern. Workshop on Multibunch Instabilities in Future Electron and Positron Accelerators (MBI-97), KEKProceedings 97-17 (1997) p.170.
- [8] M. A. Furman, LBL-41482/CBP Note 247/LHC Project Report 180, May 20, 1998.
- [9] K. Ohmi and F. Zimmermann, Phys. Rev. Lett. 85, 3821 (2000).
- [10] K. Ohmi, F. Zimmermann and E. Perevedentsev, Phys. Rev. E 65, 16502 (2002).
- [11] A. W. Chao, Physics of Collective Beam Instabilities in High Energy Accelerators, Wiley-Interscience Publication.
- [12] E. Keil and B. Zotter, CERN-ISR-TH/71-58.
- [13] S. Kato and M. Nishiwaki, section 2.3.8.2 in Accelerator Technical Design Report for High-Intensity Proton Accelerator Facility Project.
- [14] T. Toyama, KEK Internal Report, ASN-452 (in Japanese) 2001.